# Relaxation of the Courant Condition in the Explicit Finite-Difference Time-Domain Method with Higher-Degree Differential Terms

Harune Sekido and Takayuki Umeda, *Member, IEEE*

***Abstract*—A new explicit and non-dissipative FDTD method in two and three dimensions is proposed for relaxation of the Courant condition. The third-degree spatial difference terms with second- and fourth-order accuracy are added with coefficients to the time-development equations of FDTD(2,4). Optimal coefficients are obtained by a brute-force search of the dispersion relations, which reduces phase velocity errors but satisfies the numerical stability as well. The new method is stable with large Courant numbers where the conventional FDTD methods are unstable. The new method also has smaller numerical errors in the phase velocity than conventional FDTD methods with small Courant numbers.**

***Index Terms*—FDTD, Courant condition, dispersion relation, phase velocity.**

## I. Introduction

THE Finite-Difference Time-Domain (FDTD) method is a numerical method for solving the time development of electromagnetic fields [1], [2]. The time-development equations used in the FDTD method is obtained by approximating Maxwell's equations with the finite difference of second-order accuracy in both time and space. A staggered grid (Yee grid) system is used in the spatial difference so that Gauss's law for both electric and magnetic fields is always satisfied. Owing to this advantage and the simpleness of the numerical algorithm, the FDTD method has been used as the standard numerical method for electromagnetic fields for more than a half century.

Maxwell's equations are written as follows:

$$\frac{\partial \boldsymbol{B}}{\partial t} + \nabla \times \boldsymbol{E} = \boldsymbol{0} \tag{1a}$$

$$\epsilon \frac{\partial \boldsymbol{E}}{\partial t} - \frac{1}{\mu} \nabla \times \boldsymbol{B} = -\boldsymbol{J} \tag{1b}$$

$$\nabla \cdot \boldsymbol{E} = \frac{\rho}{\epsilon} \tag{1c}$$

$$\nabla \cdot \boldsymbol{B} = 0 \tag{1d}$$

where $\boldsymbol{E}$ is electric field, $\boldsymbol{B}$ is magnetic field, $\boldsymbol{J}$ is current density, $\epsilon$ is permeability, $\mu$ is permittivity, and $\rho$ is charge density.

Assuming a case in vacuum ($\boldsymbol{J} = \boldsymbol{0}$, $\rho = 0$), (1) are written in the three vector components in the rectangular coordinate system as follows:

$$-\frac{\partial B_x}{\partial t} = \frac{\partial E_z}{\partial y} - \frac{\partial E_y}{\partial z} \tag{2a}$$

$$-\frac{\partial B_y}{\partial t} = \frac{\partial E_x}{\partial z} - \frac{\partial E_z}{\partial x} \tag{2b}$$

$$-\frac{\partial B_z}{\partial t} = \frac{\partial E_y}{\partial x} - \frac{\partial E_x}{\partial y} \tag{2c}$$

$$\epsilon \frac{\partial E_x}{\partial t} = \frac{1}{\mu} \left( \frac{\partial B_z}{\partial y} - \frac{\partial B_y}{\partial z} \right) \tag{2d}$$

$$\epsilon \frac{\partial E_y}{\partial t} = \frac{1}{\mu} \left( \frac{\partial B_x}{\partial z} - \frac{\partial B_z}{\partial x} \right) \tag{2e}$$

$$\epsilon \frac{\partial E_z}{\partial t} = \frac{1}{\mu} \left( \frac{\partial B_y}{\partial x} - \frac{\partial B_x}{\partial y} \right). \tag{2f}$$

The time-development equations are derived by approximating temporal and spatial differential terms in (2) with the finite difference of second-order accuracy:

$$\begin{aligned} &B_x^{t+\frac{\Delta t}{2}} \left( x, y + \frac{\Delta y}{2}, z + \frac{\Delta z}{2} \right) \\ &= B_x^{t-\frac{\Delta t}{2}} \left( x, y + \frac{\Delta y}{2}, z + \frac{\Delta z}{2} \right) \\ &- \mathcal{D}_y^1 E_z^t \left( x, y + \frac{\Delta y}{2}, z + \frac{\Delta z}{2} \right) \\ &+ \mathcal{D}_z^1 E_y^t \left( x, y + \frac{\Delta y}{2}, z + \frac{\Delta z}{2} \right) \end{aligned} \tag{3a}$$

$$\begin{aligned} E_x^{t+\Delta t} \left( x + \frac{\Delta x}{2}, y, z \right) &= E_x^t \left( x + \frac{\Delta x}{2}, y, z \right) \\ &+ c^2 \mathcal{D}_y^1 B_z^{t-\frac{\Delta t}{2}} \left( x + \frac{\Delta x}{2}, y, z \right) \\ &- c^2 \mathcal{D}_z^1 B_y^{t-\frac{\Delta t}{2}} \left( x + \frac{\Delta x}{2}, y, z \right) \end{aligned} \tag{3b}$$

$$\begin{aligned} &B_y^{t+\frac{\Delta t}{2}} \left( x + \frac{\Delta x}{2}, y, z + \frac{\Delta z}{2} \right) \\ &= B_y^{t-\frac{\Delta t}{2}} \left( x + \frac{\Delta x}{2}, y, z + \frac{\Delta z}{2} \right) \\ &- \mathcal{D}_z^1 E_x^t \left( x + \frac{\Delta x}{2}, y, z + \frac{\Delta z}{2} \right) \\ &+ \mathcal{D}_x^1 E_z^t \left( x + \frac{\Delta x}{2}, y, z + \frac{\Delta z}{2} \right) \end{aligned} \tag{3c}$$

$$\begin{aligned} E_y^{t+\Delta t} \left( x, y + \frac{\Delta y}{2}, z \right) &= E_y^t \left( x, y + \frac{\Delta y}{2}, z \right) \\ &+ c^2 \mathcal{D}_z^1 B_x^{t-\frac{\Delta t}{2}} \left( x, y + \frac{\Delta y}{2}, z \right) \\ &- c^2 \mathcal{D}_x^1 B_z^{t-\frac{\Delta t}{2}} \left( x, y + \frac{\Delta y}{2}, z \right) \end{aligned} \tag{3d}$$

H. Sekido and T. Umeda are with Institute for Space-Earth Environmental Research, Nagoya University (e-mail: sekido@isee.nagoya-u.ac.jp).

$$
\begin{aligned}
&B_z^{t+\frac{\Delta t}{2}}\left(x+\frac{\Delta x}{2},y+\frac{\Delta y}{2},z\right)\\
&=B_z^{t-\frac{\Delta t}{2}}\left(x+\frac{\Delta x}{2},y+\frac{\Delta y}{2},z\right)\\
&-\mathcal{D}_x^1E_y^t\left(x+\frac{\Delta x}{2},y+\frac{\Delta y}{2},z\right)\\
&+\mathcal{D}_y^1E_x^t\left(x+\frac{\Delta x}{2},y+\frac{\Delta y}{2},z\right)
\end{aligned}
\tag{3e}
$$

$$
\begin{aligned}
E_z^{t+\Delta t}\left(x,y,z+\frac{\Delta z}{2}\right)&=E_z^t\left(x,y,z+\frac{\Delta z}{2}\right)\\
&+c^2\mathcal{D}_x^1B_y^{t-\frac{\Delta t}{2}}\left(x,y,z+\frac{\Delta z}{2}\right)\\
&-c^2\mathcal{D}_y^1B_x^{t-\frac{\Delta t}{2}}\left(x,y,z+\frac{\Delta z}{2}\right)
\end{aligned}
\tag{3f}
$$

where $\mathcal{D}_x^n$ is a $n$th-degree spatial difference operator. Note that $\mathcal{D}_z^n=0$ in two dimensions. Here, the speed of light $c$ is defined as $c=\sqrt{1/\epsilon\mu}$.

The first-degree spatial difference operator in the $x$ direction with the second-order accuracy $\mathcal{D}_x^1$ is defined as follows:

$$
\begin{aligned}
&\mathcal{D}_x^1E_y^t\left(x+\frac{\Delta x}{2},y+\frac{\Delta y}{2},z\right)\\
&=\frac{\Delta t}{\Delta x}\left\{E_y^t\left(x+\Delta x,y+\frac{\Delta y}{2},z\right)\right.\\
&\left.-E_y^t\left(x,y+\frac{\Delta y}{2},z\right)\right\}.
\end{aligned}
\tag{4}
$$

The FDTD method has a disadvantage that numerical oscillations occur in discontinuous waveforms and even in continuous waveforms with a large slope. The numerical oscillations are caused by an error in the phase velocity, which depends on frequency or wavenumber. To reduce the numerical error in the phase velocity, higher-order finite differences are used. The FDTD(2,4) method uses the fourth-order spatial difference [3], [4].

The first-degree spatial difference operator in the $x$ direction with the fourth-order accuracy $\mathcal{D}_x^1$ is defined as follows:

$$
\begin{aligned}
&\mathcal{D}_x^1E_y^t\left(x+\frac{\Delta x}{2},y+\frac{\Delta y}{2},z\right)\\
&=\frac{1}{24}\frac{\Delta t}{\Delta x}\left\{-E_y^t\left(x+2\Delta x,y+\frac{\Delta y}{2},z\right)\right.\\
&+27E_y^t\left(x+\Delta x,y+\frac{\Delta y}{2},z\right)-27E_y^t\left(x,y+\frac{\Delta y}{2},z\right)\\
&\left.+E_y^t\left(x-\Delta x,y+\frac{\Delta y}{2},z\right)\right\}.
\end{aligned}
\tag{5}
$$

The FDTD method using $t$th-order accuracy in time and $x$th-order accuracy in space is generally referred to as FDTD($t$,$x$).

The numerical error in the phase velocity of FDTD(2,4) is smaller than that of FDTD(2,2). However, the Courant condition of FDTD(2,4) method is more restricted than that of FDTD(2,2). In general, higher-order finite differences in space with the second-order finite difference in time make the Courant condition more restrictive, which requires smaller $\Delta t$ and larger number of time steps.

The Courant condition is derived from dispersion relation. Considering only $x$ direction in one dimension, the dispersion relation of FDTD(2,2) is derived by Fourier transform of (3) and (4) as follows:

$$
\left[\sin\left(\frac{\omega\Delta t}{2}\right)\right]^2=\left[C\sin\left(\frac{k\Delta x}{2}\right)\right]^2 \tag{6}
$$

where $C=c\Delta t/\Delta x$ is the Courant number. In the same way, the dispersion relation for FDTD(2,4) is derived from (3) with (5) as follows:

$$
\begin{aligned}
&\left[\sin\left(\frac{\omega\Delta t}{2}\right)\right]^2\\
&=\left[C\left\{\sin\left(\frac{k\Delta x}{2}\right)+\frac{1}{6}\sin^3\left(\frac{k\Delta x}{2}\right)\right\}\right]^2.
\end{aligned}
\tag{7}
$$

The right-hand sides of (6) and (7) are both maximized at $k\Delta x=\pi$:

$$
\begin{aligned}
\sin^2\left(\frac{\omega\Delta t}{2}\right)&=C^2\\
\sin^2\left(\frac{\omega\Delta t}{2}\right)&=\left(\frac{7}{6}C\right)^2.
\end{aligned}
$$

Therefore, the right-hand side of (7) is more than 1 for $C>6/7\sim0.857$, which causes a numerical instability.

Zhou et al. [5] used different operators to update electric and magnetic field. The Zhou schemes have almost the same numerical dispersion as the standard FDTD method but reduce the computational costs. However, the Courant conditions of the Zhou schemes are as restricted as the standard FDTD method.

The FDTD modified(2,4) (M(2,4)) method [6] corrects the phase velocity of FDTD(2,4) by adding a difference term which uses diagonal grid points. The second-order nonstandard (NS)-FDTD method [7], [8] reduces anisotropic errors in the phase velocity by considering diagonal differences. The numerical phase velocity is matched with the physical speed of light at a specific frequency only in this method. Furthermore, the Wideband (W)NS-FDTD method aiming for analysis in a wide frequency band corrects the phase velocity error of NS-FDTD by a post process [9]. In these methods, the phase velocity error is reduced by adding various difference terms with coefficients which corrects numerical dispersion. However, it is not easy to determine appropriate coefficients for the correction terms.

The Crank-Nicolson (CN)-FDTD method [10]–[12] and the Alternating Direction Implicit (ADI)-FDTD method [13]–[16] use implicit time-development equations which relaxes the Courant condition. However, the implicit equations have larger computational costs which are solved with the matrix inversion or iterative convergence.

This paper aims to relax the Courant condition of the FDTD(2,4) method in two and three dimensions. A new explicit and non-dissipative method is developed by adding third-degree spatial difference terms with coefficients to the time-development equations of FDTD(2,4). The coefficients are determined so that the phase velocity error is minimized but numerical instabilities are suppressed as well.

This paper is organized as follows. In section 2, the time-development equations and the dispersion relation of the new methods are shown. In section 3 and 4, the optimal coefficients, the phase velocity errors, and the results of numerical tests using the new methods in two and three dimensions are shown, respectively. In section 5, the conclusion is given.

## II. Formulation and Numerical Dispersion Relation

### A. General Form

The time-development equations with third-degree spatial difference terms are written as follows:

$$\begin{aligned}
&B_x^{t+\frac{\Delta t}{2}}\left(x, y+\frac{\Delta y}{2}, z+\frac{\Delta z}{2}\right) \\
&= B_x^{t-\frac{\Delta t}{2}}\left(x, y+\frac{\Delta y}{2}, z+\frac{\Delta z}{2}\right) \\
&- \mathcal{D}_y^1 E_z^t\left(x, y+\frac{\Delta y}{2}, z+\frac{\Delta z}{2}\right) \\
&- \alpha\mathcal{D}_y^3 E_z^t\left(x, y+\frac{\Delta y}{2}, z+\frac{\Delta z}{2}\right) \\
&+ \mathcal{D}_z^1 E_y^t\left(x, y+\frac{\Delta y}{2}, z+\frac{\Delta z}{2}\right) \\
&+ \alpha\mathcal{D}_z^3 E_y^t\left(x, y+\frac{\Delta y}{2}, z+\frac{\Delta z}{2}\right)
\end{aligned} \tag{8a}$$

$$\begin{aligned}
&E_x^{t+\Delta t}\left(x+\frac{\Delta x}{2}, y, z\right) = E_x^t\left(x+\frac{\Delta x}{2}, y, z\right) \\
&+ c^2\mathcal{D}_y^1 B_z^{t-\frac{\Delta t}{2}}\left(x+\frac{\Delta x}{2}, y, z\right) \\
&+ c^2\alpha\mathcal{D}_y^3 B_z^{t-\frac{\Delta t}{2}}\left(x+\frac{\Delta x}{2}, y, z\right) \\
&- c^2\mathcal{D}_z^1 B_y^{t-\frac{\Delta t}{2}}\left(x+\frac{\Delta x}{2}, y, z\right) \\
&- c^2\alpha\mathcal{D}_z^3 B_y^{t-\frac{\Delta t}{2}}\left(x+\frac{\Delta x}{2}, y, z\right)
\end{aligned} \tag{8b}$$

$$\begin{aligned}
&B_y^{t+\frac{\Delta t}{2}}\left(x+\frac{\Delta x}{2}, y, z+\frac{\Delta z}{2}\right) \\
&= B_y^{t-\frac{\Delta t}{2}}\left(x+\frac{\Delta x}{2}, y, z+\frac{\Delta z}{2}\right) \\
&- \mathcal{D}_z^1 E_x^t\left(x+\frac{\Delta x}{2}, y, z+\frac{\Delta z}{2}\right) \\
&- \alpha\mathcal{D}_z^3 E_x^t\left(x+\frac{\Delta x}{2}, y, z+\frac{\Delta z}{2}\right) \\
&+ \mathcal{D}_x^1 E_z^t\left(x+\frac{\Delta x}{2}, y, z+\frac{\Delta z}{2}\right) \\
&+ \alpha\mathcal{D}_x^3 E_z^t\left(x+\frac{\Delta x}{2}, y, z+\frac{\Delta z}{2}\right)
\end{aligned} \tag{8c}$$

$$\begin{aligned}
&E_y^{t+\Delta t}\left(x, y+\frac{\Delta y}{2}, z\right) = E_y^t\left(x, y+\frac{\Delta y}{2}, z\right) \\
&+ c^2\mathcal{D}_z^1 B_x^{t-\frac{\Delta t}{2}}\left(x, y+\frac{\Delta y}{2}, z\right) \\
&+ \alpha c^2\mathcal{D}_z^3 B_x^{t-\frac{\Delta t}{2}}\left(x, y+\frac{\Delta y}{2}, z\right) \\
&- c^2\mathcal{D}_x^1 B_z^{t-\frac{\Delta t}{2}}\left(x, y+\frac{\Delta y}{2}, z\right) \\
&- \alpha c^2\mathcal{D}_x^3 B_z^{t-\frac{\Delta t}{2}}\left(x, y+\frac{\Delta y}{2}, z\right)
\end{aligned} \tag{8d}$$

$$\begin{aligned}
&B_z^{t+\frac{\Delta t}{2}}\left(x+\frac{\Delta x}{2}, y+\frac{\Delta y}{2}, z\right) \\
&= B_z^{t-\frac{\Delta t}{2}}\left(x+\frac{\Delta x}{2}, y+\frac{\Delta y}{2}, z\right) \\
&- \mathcal{D}_x^1 E_y^t\left(x+\frac{\Delta x}{2}, y+\frac{\Delta y}{2}, z\right) \\
&- \alpha\mathcal{D}_x^3 E_y^t\left(x+\frac{\Delta x}{2}, y+\frac{\Delta y}{2}, z\right) \\
&+ \mathcal{D}_y^1 E_x^t\left(x+\frac{\Delta x}{2}, y+\frac{\Delta y}{2}, z\right) \\
&+ \alpha\mathcal{D}_y^3 E_x^t\left(x+\frac{\Delta x}{2}, y+\frac{\Delta y}{2}, z\right)
\end{aligned} \tag{8e}$$

$$\begin{aligned}
&E_z^{t+\Delta t}\left(x, y, z+\frac{\Delta z}{2}\right) = E_z^t\left(x, y, z+\frac{\Delta z}{2}\right) \\
&+ c^2\mathcal{D}_x^1 B_y^{t-\frac{\Delta t}{2}}\left(x, y, z+\frac{\Delta z}{2}\right) \\
&+ \alpha c^2\mathcal{D}_x^3 B_y^{t-\frac{\Delta t}{2}}\left(x, y, z+\frac{\Delta z}{2}\right) \\
&- c^2\mathcal{D}_y^1 B_x^{t-\frac{\Delta t}{2}}\left(x, y, z+\frac{\Delta z}{2}\right) \\
&- \alpha c^2\mathcal{D}_y^3 B_x^{t-\frac{\Delta t}{2}}\left(x, y, z+\frac{\Delta z}{2}\right)
\end{aligned} \tag{8f}$$

where a coefficient $\alpha$ is added to the third-degree difference terms. The optimal coefficient $\alpha$ depends on the Courant number $C$. The time-development (8) is based on the Taylor series of the central difference equation in time. In the present study, odd-degree difference terms are added only, because even-degree difference terms lead to a numerical dissipation.

The first-degree spatial difference with the fourth-order accuracy (5) is used for the operator $\mathcal{D}_x^1$. The third-degree spatial difference with the second- and fourth-order accuracy are also used for the operator $\mathcal{D}_x^3$ as shown below.

### B. Second-order

The third-degree difference operator with the second-order accuracy $\mathcal{D}_x^3$ is defined as follows:

$$\begin{aligned}&\mathcal{D}_x^3 E_y^t\left(x+\frac{\Delta x}{2}, y+\frac{\Delta y}{2}, z\right)\\&=c^2\left(\frac{\Delta t}{\Delta x}\right)^3\left\{E_y^t\left(x+2\Delta x, y+\frac{\Delta y}{2}, z\right)\right.\\&-3E_y^t\left(x+\Delta x, y+\frac{\Delta y}{2}, z\right)+3E_y^t\left(x, y+\frac{\Delta y}{2}, z\right)\\&\left.-E_y^t\left(x-\Delta x, y+\frac{\Delta y}{2}, z\right)\right\}.\end{aligned} \tag{9}$$

The following dispersion relation is derived by Fourier transform of the time-development (8) with (5) and (9):

$$\begin{aligned}\mathcal{W}^2=&16\alpha^2\left(C_x^6\mathcal{K}_x^6+C_y^6\mathcal{K}_y^6+C_z^6\mathcal{K}_z^6\right)\\&-2\alpha\left\{4\left(C_x^4\mathcal{K}_x^4+C_y^4\mathcal{K}_y^4+C_z^4\mathcal{K}_z^4\right)\right.\\&\left.+\frac{2}{3}\left(C_x^4\mathcal{K}_x^6+C_y^4\mathcal{K}_y^6+C_z^4\mathcal{K}_z^6\right)\right\}\\&+\left\{\left(C_x^2\mathcal{K}_x^2+C_y^2\mathcal{K}_y^2+C_z^2\mathcal{K}_z^2\right)\right.\\&+\frac{1}{3}\left(C_x^2\mathcal{K}_x^4+C_y^2\mathcal{K}_y^4+C_z^2\mathcal{K}_z^4\right)\\&\left.+\frac{1}{36}\left(C_x^2\mathcal{K}_x^6+C_y^2\mathcal{K}_y^6+C_z^2\mathcal{K}_z^6\right)\right\}\end{aligned} \tag{10}$$

where $\mathcal{W}=\sin\left(\frac{\omega\Delta t}{2}\right)$ and $\mathcal{K}_x=\sin\left(\frac{k_x\Delta x}{2}\right)$. Note that $\mathcal{K}_z=0$ in two dimensions. The Courant number is defined as $C_x=c\Delta t/\Delta x$, $C_y=c\Delta t/\Delta y$, and $C_z=c\Delta t/\Delta z$. A possible range of the left-hand side is $0\le\mathcal{W}^2\le 1$. For $\alpha=0$ and $\Delta x=\Delta y=\Delta z$ (i.e., $C=C_x=C_y=C_z$), the Courant condition is not satisfied in the range of $C\ge 6/7\sqrt{2}\sim 0.61$ in two dimensions and $C\ge 6/7\sqrt{3}\sim 0.49$ in three dimensions. Since the second term on the right-hand side of (10) has a negative sign, the Courant condition can be relaxed by adjusting the coefficient $\alpha$.

We call this method "scheme 1" in this paper.

### C. Fourth-order

The third-degree difference operator with the fourth-order accuracy $\mathcal{D}_x^3$ is defined as follows:

$$\begin{aligned}&\mathcal{D}_x^3 E_y^t\left(x+\frac{\Delta x}{2}, y+\frac{\Delta y}{2}, z\right)\\&=\frac{c^2}{8}\left(\frac{\Delta t}{\Delta x}\right)^3\left\{-E_y^t\left(x+3\Delta x, y+\frac{\Delta y}{2}, z\right)\right.\\&+13E_y^t\left(x+2\Delta x, y+\frac{\Delta y}{2}, z\right)\\&-34E_y^t\left(x+\Delta x, y+\frac{\Delta y}{2}, z\right)\\&+34E_y^t\left(x, y+\frac{\Delta y}{2}, z\right)\\&-13E_y^t\left(x-\Delta x, y+\frac{\Delta y}{2}, z\right)\\&\left.+E_y^t\left(x-2\Delta x, y+\frac{\Delta y}{2}, z\right)\right\}.\end{aligned} \tag{11}$$

The following dispersion relation is derived by Fourier transform of the time-development (8) with (5) and (11):

$$\begin{aligned}\mathcal{W}^2=&\alpha^2\left\{16\left(C_x^6\mathcal{K}_x^6+C_y^6\mathcal{K}_y^6+C_z^6\mathcal{K}_z^6\right)\right.\\&+16\left(C_x^6\mathcal{K}_x^8+C_y^6\mathcal{K}_y^8+C_z^6\mathcal{K}_z^8\right)\\&\left.+4\left(C_x^6\mathcal{K}_x^{10}+C_y^6\mathcal{K}_y^{10}+C_z^6\mathcal{K}_z^{10}\right)\right\}\\&-2\alpha\left\{4\left(C_x^4\mathcal{K}_x^4+C_y^4\mathcal{K}_y^4+C_z^4\mathcal{K}_z^4\right)\right.\\&+\frac{8}{3}\left(C_x^4\mathcal{K}_x^6+C_y^4\mathcal{K}_y^6+C_z^4\mathcal{K}_z^6\right)\\&\left.+\frac{1}{3}\left(C_x^4\mathcal{K}_x^8+C_y^4\mathcal{K}_y^8+C_z^4\mathcal{K}_z^8\right)\right\}\\&+\left\{\left(C_x^2\mathcal{K}_x^2+C_y^2\mathcal{K}_y^2+C_z^2\mathcal{K}_z^2\right)\right.\\&+\frac{1}{3}\left(C_x^2\mathcal{K}_x^4+C_y^2\mathcal{K}_y^4+C_z^2\mathcal{K}_z^4\right)\\&\left.+\frac{1}{36}\left(C_x^2\mathcal{K}_x^6+C_y^2\mathcal{K}_y^6+C_z^2\mathcal{K}_z^6\right)\right\}.\end{aligned} \tag{12}$$

Note that $\mathcal{K}_z=0$ in two dimensions.

We call this method "scheme 2" in this paper.

## III. Two Dimensions

### A. Optimal Coefficients

A brute-force search is performed to find an optimal coefficient for the third-degree spatial difference term that minimizes the numerical error in the phase velocity and suppresses the numerical instability. The phase velocity is obtained by solving the dispersion relation for the angular frequency $\omega$ and dividing the real part of $\omega$ by the wavenumber $k$. In the present study, we assume $\Delta x=\Delta y=\Delta z$ (i.e., $C=C_x=C_y=C_z$). The error is calculated by the following equation:

$$\varepsilon=\frac{1}{\pi^3 c}\sqrt{\int_0^\pi\int_0^\pi\int_0^\pi\left\{\frac{\omega(k_x,k_y,k_z)}{\sqrt{k_x^2+k_y^2+k_z^2}}-c\right\}^2\mathrm{d}k_x\mathrm{d}k_y\mathrm{d}k_z}. \tag{13}$$

The results of the coefficients search for scheme 1 in the range of $0.5\le C\le 1$ using (10) are shown in Table I. The results of the coefficients search for scheme 2 in the range of $0.5\le C\le 1$ using (12) are shown in Table II.

The present method is useful to the Courant number $C>1$ as well. In the present study, however, the coefficients are searched in the range of $C\le 1$ because the numerical error increases as the Courant number $C$ increases as shown in the next subsection.

### B. Numerical Error

The phase velocity errors of the scheme 1 and 2 are compared against those of FDTD(2,2) and FDTD(2,4). Figure 1 shows that the phase velocity error averaged over the entire wavenumber space. The horizontal axis is the Courant number $C$ and the vertical axis is the relative error $\varepsilon$ of the phase velocity to $C$.

Figure 1 shows that the phase velocity errors of the new methods are smaller than those of the conventional methods. The numerical instability is also suppressed for $C\le 1$. The numerical errors of the scheme 2 are smaller than those of scheme 1 for most Courant numbers.

TABLE I: Optimal Coefficients in the Two-Dimensional Scheme 1.

| $C$ | $\alpha$ | $C$ | $\alpha$ |
|---|---|---|---|
| 0.50 | -0.0505 | 0.76 | 0.1023 |
| 0.51 | -0.0428 | 0.77 | 0.1048 |
| 0.52 | -0.0354 | 0.78 | 0.1069 |
| 0.53 | -0.0284 | 0.79 | 0.1088 |
| 0.54 | -0.0216 | 0.80 | 0.1105 |
| 0.55 | -0.0152 | 0.81 | 0.112 |
| 0.56 | -0.0089 | 0.82 | 0.1132 |
| 0.57 | -0.0029 | 0.83 | 0.1143 |
| 0.58 | 0.003 | 0.84 | 0.1152 |
| 0.59 | 0.0087 | 0.85 | 0.1159 |
| 0.60 | 0.0144 | 0.86 | 0.1165 |
| 0.61 | 0.0201 | 0.87 | 0.1169 |
| 0.62 | 0.0258 | 0.88 | 0.1173 |
| 0.63 | 0.0318 | 0.89 | 0.1175 |
| 0.64 | 0.0383 | 0.90 | 0.1176 |
| 0.65 | 0.0467 | 0.91 | 0.1177 |
| 0.66 | 0.0547 | 0.92 | 0.1176 |
| 0.67 | 0.062 | 0.93 | 0.1175 |
| 0.68 | 0.0686 | 0.94 | 0.1173 |
| 0.69 | 0.0745 | 0.95 | 0.117 |
| 0.70 | 0.0799 | 0.96 | 0.1167 |
| 0.71 | 0.0847 | 0.97 | 0.1163 |
| 0.72 | 0.0891 | 0.98 | 0.1159 |
| 0.73 | 0.093 | 0.99 | 0.1155 |
| 0.74 | 0.0964 | 1.00 | 0.1149 |
| 0.75 | 0.0995 | | |

TABLE II: Optimal Coefficients in the Two-Dimensional Scheme 2.

| $C$ | $\alpha$ | $C$ | $\alpha$ |
|---|---|---|---|
| 0.50 | -0.0372 | 0.76 | 0.0682 |
| 0.51 | -0.0316 | 0.77 | 0.07 |
| 0.52 | -0.0262 | 0.78 | 0.0713 |
| 0.53 | -0.0211 | 0.79 | 0.0727 |
| 0.54 | -0.0162 | 0.80 | 0.0737 |
| 0.55 | -0.0117 | 0.81 | 0.0747 |
| 0.56 | -0.0071 | 0.82 | 0.0755 |
| 0.57 | -0.0029 | 0.83 | 0.0762 |
| 0.58 | 0.0014 | 0.84 | 0.0769 |
| 0.59 | 0.0056 | 0.85 | 0.0774 |
| 0.60 | 0.0095 | 0.86 | 0.0778 |
| 0.61 | 0.0135 | 0.87 | 0.078 |
| 0.62 | 0.0176 | 0.88 | 0.0783 |
| 0.63 | 0.0216 | 0.89 | 0.0784 |
| 0.64 | 0.026 | 0.90 | 0.0784 |
| 0.65 | 0.0312 | 0.91 | 0.0785 |
| 0.66 | 0.0366 | 0.92 | 0.0784 |
| 0.67 | 0.0414 | 0.93 | 0.0784 |
| 0.68 | 0.0459 | 0.94 | 0.0783 |
| 0.69 | 0.0498 | 0.95 | 0.0781 |
| 0.70 | 0.0533 | 0.96 | 0.078 |
| 0.71 | 0.0565 | 0.97 | 0.0779 |
| 0.72 | 0.0594 | 0.98 | 0.0778 |
| 0.73 | 0.0621 | 0.99 | 0.0778 |
| 0.74 | 0.0644 | 1.00 | 0.0776 |
| 0.75 | 0.0664 | | |

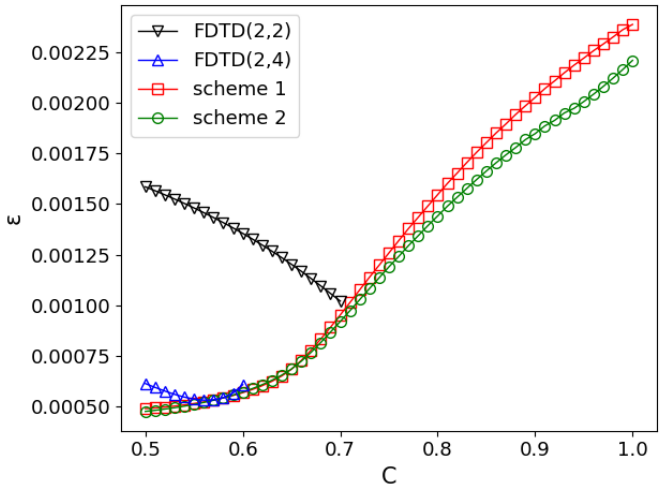


Fig. 1: Comparison of phase velocity errors averaged over the entire wavenumber space in two dimensions.

Figure 2 shows that the phase velocity errors for specific propagation angles $\theta$. Here, $\theta$ is the angle from the $x$ axis. Panels (a) and (b) show the numerical errors at $\theta = 0°$ and $\theta = 45°$, respectively. The numerical errors in Panels (a) and (b) are obtained by averaging over $k_y = 0$ and $k_x = k_y$ axes, respectively. The horizontal axis is the Courant number $C$ and the vertical axis is the relative error $\varepsilon$ of the phase velocity to $C$. Note that the dispersion relation is symmetric with respect to the $|k_x| = |k_y|$ axis.

Figure 2 shows that the numerical errors at $\theta = 45°$ are smaller than those at $\theta = 0°$. For $C > 0.7$, the numerical errors at $\theta = 45°$ are smaller than the half of those at $\theta = 0°$.

### C. Numerical Results

Numerical simulations are performed with $c = 10.0$, $\Delta x = \Delta y = 1.0$, and $\Delta t = C\Delta x/c$. The number of grid points is $N_x = N_y = 440$. The following current density is imposed to emit an electromagnetic pulse with $\tau = 0.25$ at the center of the simulation domain:

$$
\begin{aligned}
J_x\left(x = \frac{\Delta x}{2}, y = 0, z = 0, t\right) &= \cosh^{-2}\left(\frac{t-4}{2\tau}\right) \\
J_x\left(x = \frac{\Delta x}{2}, y = \Delta y, z = 0, t\right) &= -\cosh^{-2}\left(\frac{t-4}{2\tau}\right) \\
J_y\left(x = \Delta x, y = \frac{\Delta y}{2}, z = 0, t\right) &= \cosh^{-2}\left(\frac{t-4}{2\tau}\right) \\
J_y\left(x = 0, y = \frac{\Delta y}{2}, z = 0, t\right) &= -\cosh^{-2}\left(\frac{t-4}{2\tau}\right).
\end{aligned}
\tag{14}
$$

Periodic boundaries are used as the boundary conditions in both $x$ and $y$ directions.

The results of numerical simulations are shown in Figure 3. Panels (a), (b), (c), (d), (e) and (f) show the spatial profile of the magnetic field $B_z$ contentment with FDTD(2,2) and

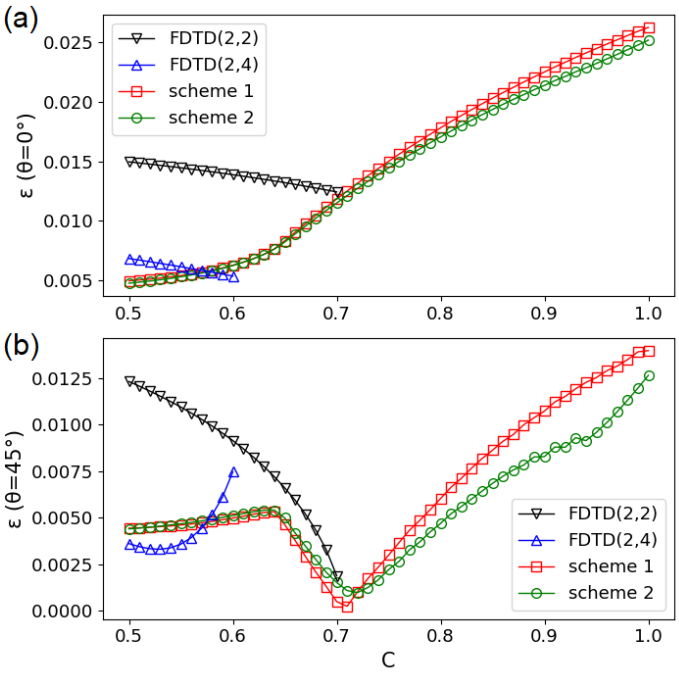


Fig. 2: Comparisons of phase velocity errors averaged over the specific directional wavenumber space in two dimensions: (a) $\theta = 0°$; (b) $\theta = 45°$.

$C = 0.5$, FDTD(2,4) and $C = 0.5$, scheme 1 and $C = 0.5$, scheme 2 and $C = 0.5$, scheme 1 and $C = 1$, and scheme 2 and $C = 1$, respectively.

With the Courant number $C = 0.5$, numerical oscillations are observed at the rear of the pulse with FDTD(2,2). The input pulse consists of multiple wavenumber components. Therefore, the differences between the theoretical speed of light and numerical phase velocities, which depends on wavenumber, are appeared as numerical oscillations. With FDTD(2,2), the numerical oscillations with small wavenumbers appear at the rear of the pulse because phase velocities of modes with large wave numbers are small. The numerical oscillations are not observed with FDTD(2,4), schemes 1 and 2. Figures 1 and 2 show that the numerical error with FDTD(2,2) is more than twice as large as that with other schemes. Therefore, these numerical simulations are consistent with the dispersion relations which shows the dependence of phase velocity errors on wavenumbers.

With $C = 1$, the numerical simulations are unstable with conventional FDTD(2,2) and FDTD(2,4) due to the Courant condition. However, the numerical simulations are stable with both schemes 1 and 2. The numerical oscillations with scheme 2 is smaller than those with scheme 1. The numerical oscillations are the smallest at $\theta = 45°$ and the largest at $\theta = 0°$. This is consistent with Figure 2 which shows that the phase velocity errors at $\theta = 45°$ are smaller than those at $\theta = 0°$.

The computational time of the simulations is shown in Table III. The computational time is measured on a single core of the Intel Xeon Gold 6230R processor. The Intel Fortran compiler Version 2021.5.0 is used with options of "-ipo -ip -O3 -xCASCADELAKE".

TABLE III: Computational Time in the Two Dimensions.

| | $C = 0.5$ | $C = 1$ |
|---|---|---|
| FDTD(2,2) | 1.39656301468611 | - |
| FDTD(2,4) | 1.45807087451220 | - |
| scheme 1 | 1.51422649439424 | 0.756914421655238 |
| scheme 2 | 1.76735660718754 | 0.888097147289664 |

The computational time at the same Courant number increases as the number of operations increases. With $C = 0.5$, the computational time with schemes 1 and 2 are 1.04 and 1.21 times longer than that with FDTD(2,4), respectively, although the schemes 1 and 2 have 2 and 2.5 times larger number of operations than FDTD(2,4), respectively. The computational time is given by the sum of the processing time of floating-point operations and the memory access time. Since the computational cost of memory access is higher than floating-point operations, the computational time is not proportional to the number of operations. Furthermore, the computational time with $C = 1$ is a half of that with $C = 0.5$. Hence, the computational time of schemes 1 and 2 with $C = 1$ is shorter than that of FDTD(2,2) and FDTD(2,4) with $C = 0.5$.

## IV. Three Dimensions

### A. Optimal Coefficients

In three dimensions, the FDTD(2,4) is unstable for $C \geq 2\sqrt{3}/7 \sim 0.49$. Therefore, optimal coefficients are searched in the range of $0.4 \leq C \leq 1$. The results of the coefficients search for scheme 1 using (10) are shown in Table IV. The results of the coefficients search for scheme 2 using (12) are shown in Table V.

### B. Numerical Error

The phase velocity errors of the schemes 1 and 2 are compared against those of FDTD(2,2) and FDTD(2,4). Figure 4 shows that the phase velocity error averaged over the entire wavenumber space. The horizontal axis is the Courant number $C$ and the vertical axis is the relative error $\varepsilon$ of the phase velocity to $C$.

Figure 4 shows that the phase velocity errors of the new methods are smaller than those of the conventional methods. The numerical instability is also suppressed for $0.5 \leq C \leq 1$. The numerical errors of the scheme 2 are smaller than those of scheme 1 for $C \lesssim 0.9$ but are larger for $C \gtrsim 0.9$.

Figure 5 shows that the numerical errors for the specific propagation angles $\theta$ and $\phi$. Here, $\theta$ is zenith angle, and $\phi$ is azimuth angle. Panels (a), (b) and (c) show the numerical errors at $(\theta, \phi) = (0°, 0°)$, $(\theta, \phi) = (45°, 0°)$ and $(\theta, \phi) = (45°, 45°)$, respectively. The numerical errors in Panels (a), (b) and (c) are obtained by averaging over $k_y = k_z = 0$ axis, $k_x = k_y, k_z = 0$ axis and $k_x = k_y = k_z$ axis, respectively. The horizontal axis is the Courant number $C$ and the vertical axis is the relative error $\varepsilon$ of the phase velocity to $C$. Note that the dispersion relation is symmetric with respect to the $|k_x| = |k_y| = |k_z|$ axis.

Figure 5 shows that the numerical errors at $(\theta, \phi) = (45°, 45°)$ are smaller than those at $(\theta, \phi) = (0°, 0°)$ and

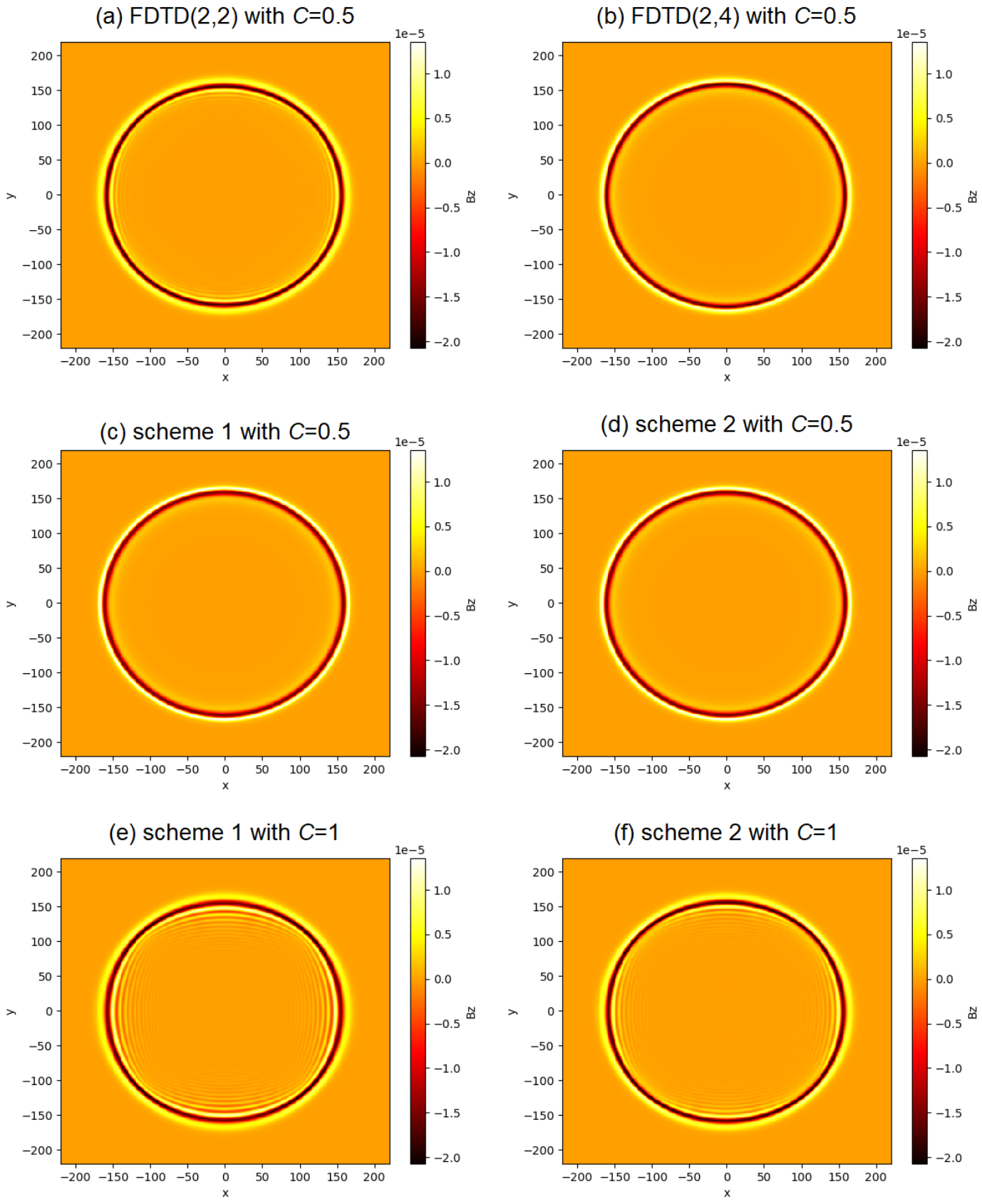


Fig. 3: Spatial profiles of $B_z$ at $t = 200\Delta t/C$ in two dimensions: (a) FDTD(2,2) with $C = 0.5$; (b) FDTD(2,4) with $C = 0.5$; (c) scheme 1 with $C = 0.5$; (d) scheme 2 with $C = 0.5$; (e) scheme 1 with $C = 1$; (f) scheme 2 with $C = 1$.

TABLE IV: Optimal Coefficients in the Three-Dimensional Scheme 1.

| $C$ | $\alpha$ | $C$ | $\alpha$ |
|---|---|---|---|
| 0.40 | -0.1147 | 0.71 | 0.1754 |
| 0.41 | -0.0992 | 0.72 | 0.176 |
| 0.42 | -0.0848 | 0.73 | 0.1763 |
| 0.43 | -0.0712 | 0.74 | 0.1765 |
| 0.44 | -0.0584 | 0.75 | 0.1764 |
| 0.45 | -0.0462 | 0.76 | 0.1762 |
| 0.46 | -0.0345 | 0.77 | 0.1758 |
| 0.47 | -0.0233 | 0.78 | 0.1753 |
| 0.48 | -0.0123 | 0.79 | 0.1746 |
| 0.49 | -0.0014 | 0.80 | 0.1739 |
| 0.50 | 0.012 | 0.81 | 0.173 |
| 0.51 | 0.0333 | 0.82 | 0.172 |
| 0.52 | 0.0522 | 0.83 | 0.171 |
| 0.53 | 0.0689 | 0.84 | 0.1699 |
| 0.54 | 0.0836 | 0.85 | 0.1687 |
| 0.55 | 0.0967 | 0.86 | 0.1675 |
| 0.56 | 0.1082 | 0.87 | 0.1662 |
| 0.57 | 0.1184 | 0.88 | 0.165 |
| 0.58 | 0.1273 | 0.89 | 0.1638 |
| 0.59 | 0.1351 | 0.90 | 0.1626 |
| 0.60 | 0.142 | 0.91 | 0.1615 |
| 0.61 | 0.148 | 0.92 | 0.1604 |
| 0.62 | 0.1532 | 0.93 | 0.1593 |
| 0.63 | 0.1577 | 0.94 | 0.1583 |
| 0.64 | 0.1615 | 0.95 | 0.1573 |
| 0.65 | 0.1648 | 0.96 | 0.1564 |
| 0.66 | 0.1676 | 0.97 | 0.1554 |
| 0.67 | 0.1699 | 0.98 | 0.1545 |
| 0.68 | 0.1718 | 0.99 | 0.1537 |
| 0.69 | 0.1733 | 1.00 | 0.1528 |
| 0.70 | 0.1745 | | |

TABLE V: Optimal Coefficients in the Three-Dimensional Scheme 2.

| $C$ | $\alpha$ | $C$ | $\alpha$ |
|---|---|---|---|
| 0.40 | -0.0863 | 0.71 | 0.1169 |
| 0.41 | -0.075 | 0.72 | 0.1173 |
| 0.42 | -0.0644 | 0.73 | 0.1176 |
| 0.43 | -0.0544 | 0.74 | 0.1177 |
| 0.44 | -0.045 | 0.75 | 0.1176 |
| 0.45 | -0.0361 | 0.76 | 0.1175 |
| 0.46 | -0.0275 | 0.77 | 0.1173 |
| 0.47 | -0.0192 | 0.78 | 0.1171 |
| 0.48 | -0.0111 | 0.79 | 0.1168 |
| 0.49 | -0.003 | 0.80 | 0.1166 |
| 0.50 | 0.0082 | 0.81 | 0.1165 |
| 0.51 | 0.0224 | 0.82 | 0.1163 |
| 0.52 | 0.0349 | 0.83 | 0.1161 |
| 0.53 | 0.046 | 0.84 | 0.1159 |
| 0.54 | 0.0559 | 0.85 | 0.1158 |
| 0.55 | 0.0646 | 0.86 | 0.1156 |
| 0.56 | 0.0722 | 0.87 | 0.1155 |
| 0.57 | 0.079 | 0.88 | 0.1153 |
| 0.58 | 0.0849 | 0.89 | 0.1152 |
| 0.59 | 0.0902 | 0.90 | 0.1151 |
| 0.60 | 0.0947 | 0.91 | 0.1149 |
| 0.61 | 0.0987 | 0.92 | 0.1148 |
| 0.62 | 0.1022 | 0.93 | 0.1147 |
| 0.63 | 0.1052 | 0.94 | 0.1146 |
| 0.64 | 0.1077 | 0.95 | 0.1145 |
| 0.65 | 0.1099 | 0.96 | 0.1144 |
| 0.66 | 0.1117 | 0.97 | 0.1143 |
| 0.67 | 0.1133 | 0.98 | 0.1142 |
| 0.68 | 0.1145 | 0.99 | 0.1141 |
| 0.69 | 0.1156 | 1.00 | 0.114 |
| 0.70 | 0.1163 | | |

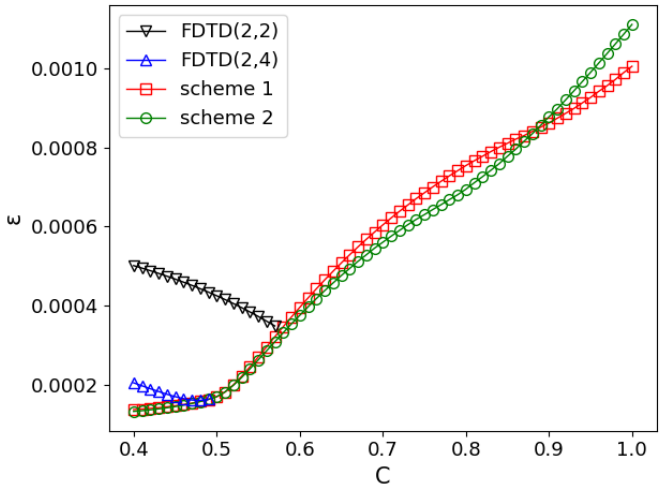


Fig. 4: Comparison of phase velocity errors averaged over the entire wavenumber space in three dimensions.

$(\theta, \phi) = (45°, 0°)$. At around $C = 0.6$, the numerical errors with schemes 1 and 2 at $(\theta, \phi) = (45°, 45°)$ are smaller than the half of those at $(\theta, \phi) = (0°, 0°)$ and $(\theta, \phi) = (45°, 0°)$.

### C. Numerical Results

Numerical simulations are performed with $c = 10.0$, $\Delta x = \Delta y = \Delta z = 1.0$, and $\Delta t = C\Delta x/c$. The number of grid points is $N_x = N_y = N_z = 440$. The current density in (14) is imposed to emit an electromagnetic pulse with $\tau = 0.25$ at the center of the simulation domain. Periodic boundaries are used as the boundary conditions in all the $x$, $y$ and $z$ directions.

The results of numerical simulations are shown in Figure 6. Panels (a), (b), (c), (d), (e) and (f) show the spatial profile of the magnetic field $B_z$ contentment with FDTD(2,2) and $C = 0.4$, FDTD(2,4) and $C = 0.4$, scheme 1 and $C = 0.4$, scheme 2 and $C = 0.4$, scheme 1 and $C = 1$, and scheme 2 and $C = 1$, respectively.

With Courant number $C = 0.4$, numerical oscillations are observed at the rear of the pulse with FDTD(2,2). The numerical oscillations are not observed with FDTD(2,4), schemes 1 and 2. Figures 4 and 5 show that the numerical error with FDTD(2,2) is more than twice as large as the numerical errors with other schemes.

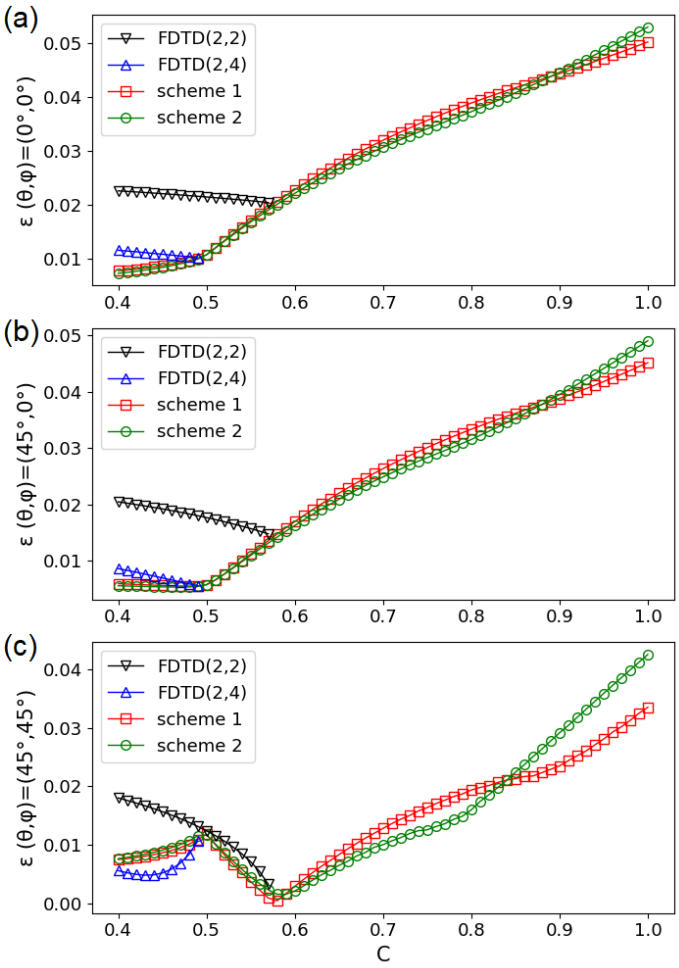


Fig. 5: Comparisons of phase velocity errors averaged over the specific directional wavenumber space in three dimensions: (a) $(\theta, \phi) = (0°, 0°)$; (b) $(\theta, \phi) = (45°, 0°)$; (c) $(\theta, \phi) = (45°, 45°)$.

With $C = 1$, the numerical simulations are unstable with conventional FDTD(2,2) and FDTD(2,4) due to the Courant condition. However, the numerical simulations are stable with both schemes 1 and 2. The numerical oscillations are the smallest at $(\theta, \phi) = (45°, 45°)$ but larger at $(\theta, \phi) = (0°, 0°)$ and $(45°, 0°)$. This is consistent with Figure 5 which shows that the phase velocity errors at $(\theta, \phi) = (45°, 45°)$ are smaller than those at $(\theta, \phi) = (0°, 0°)$ and $(45°, 0°)$.

The computational time of the simulations is shown in Table VI. The computational time is measured on the same processor and compiler as those in two dimensions.

The computational time at the same Courant number increases as the number of operations increases. With $C = 0.4$, the computational time with schemes 1 and 2 are 1.002 and 1.273 times longer than that with FDTD(2,4), respectively, although the schemes 1 and 2 have 2 and 2.5 times larger number of operations than FDTD(2,4), respectively. The computational time with $C = 1$ is 0.4 times shorter than that with $C = 0.4$. The computational time with schemes 1 and 2 at $C = 1$ is shorter than that with FDTD(2,2) and FDTD(2,4) at $C = 0.4$.

TABLE VI: Computational Time in the Three Dimensions.

| | $C = 0.4$ | $C = 1$ |
|---|---|---|
| FDTD(2,2) | 35.9662997193634 | - |
| FDTD(2,4) | 49.2364173122495 | - |
| scheme 1 | 49.3584364675544 | 19.7688133916073 |
| scheme 2 | 62.6550961998291 | 24.9873576161452 |

## V. Conclusion

A new explicit and non-dissipative FDTD method is developed to relax the Courant condition. In the conventional FDTD method, the Courant conditions are more restricted with higher order of accuracy and larger number of dimensions. In the present study, third-degree spatial difference terms with second- and fourth-order accuracy are added with coefficients to the time-development equations of FDTD(2,4) [3], [4].

Optimal coefficients are searched by using the dispersion relations, which minimize the phase velocity errors averaged over the entire wavenumber space. The present method is stable with large Courant numbers up to $C = 1$, although numerical oscillations remain. With small Courant numbers, phase velocity errors are reduced with respect to the conventional FDTD(2,4) method. The computational time with the present method at $C = 1$ is shorter than that with the conventional methods $C = 0.5$ in the two dimensions and $C = 0.4$ in the three dimensions. Hence, the present method is also useful to reduce the computational time by using a large Courant number.

In the conventional NS-FDTD method [7], [8], the diagonal spatial difference terms are added with coefficients to reduce anisotropic errors. However, an optimal coefficient is determined for a single frequency only. In the present method, optimal coefficients are determined to minimize the numerical error in the phase velocity averaged over the entire wavenumber space. Hence, the present method is useful for a wideband frequency range without post processes as well as for a nonlinear medium unlike the WNS-FDTD [9].

In the Zhou schemes [5], different operators are used to update electric and magnetic field. These schemes have smaller computational costs than the standard FDTD(2,4) and (2,6) schemes. The numerical errors of the Zhou(2,8) scheme are smaller than the FDTD(2,4)/(2,6) and Zhou(2,4)/(2,6) schemes. However, the Courant conditions of the Zhou schemes are as restricted as the standard FDTD schemes. On the other hand, the phase velocity errors with the present schemes averaged over the entire wavenumber space are smaller than those of Zhou(2,8) for $C < 0.4$ (not shown). Furthermore, the present schemes relax the Courant conditions.

Zhou et al. [5] showed that the phase velocity errors are reduced by using higher-order difference operators. Extension of the present schemes to FDTD(2,6) and (2,8) is left as future studies.

## Acknowledgements

This work was supported by MEXT/JSPS under Grant-In-Aid (KAKENHI) for Scientific Research (B) No.JP19H01868. Computations of this work were performed on the CIDAS

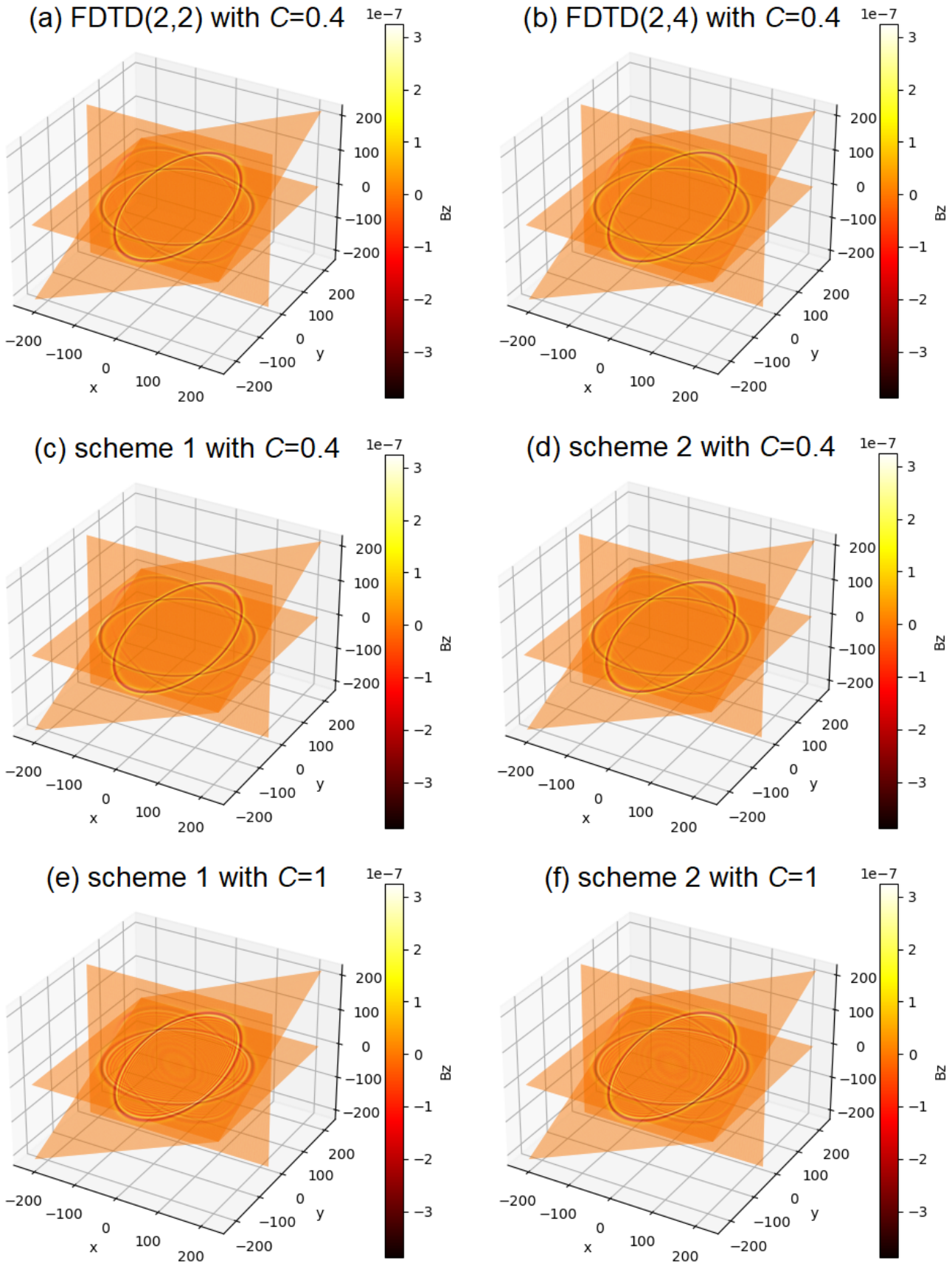


Fig. 6: Spatial profiles of $B_z$ at $t = 200\Delta t/C$ in three dimensions: (a) FDTD(2,2) with $C = 0.4$; (b) FDTD(2,4) with $C = 0.4$; (c) scheme 1 with $C = 0.4$; (d) scheme 2 with $C = 0.4$; (e) scheme 1 with $C = 1$; (f) scheme 2 with $C = 1$.

computer system at the Institute for Space-Earth Environmental Research, Nagoya University as a computational joint research program.

## REFERENCES

[1] K. S. Yee, "Numerical solution of initial boundary value problems involving Maxwell's equations in isotropic media," *IEEE Transactions on Antennas and Propagation*, vol. AP-14, no. 3, pp. 302–307, 1966.
[2] A. Taflove, "Application of the finite-difference time-domain method to sinusoidal steady-state electromagnetic-penetration problems," *IEEE Transactions on Electromagnetic Compatibility*, vol. EMC-22, no. 3, pp. 191–202, 1980.
[3] J. Fang, "Time domain finite difference computations for Maxwell's equations," Ph.D. dissertation, Dept. of Elec. Eng., Univ. of California, Berkeley, CA, 1989.
[4] P. G. Petropoulos, "Phase error control for FD-TD methods of second and fourth order accuracy," *IEEE Transactions on Antennas and Propagation*, vol. 42, no. 6, pp. 859–862, 1994.
[5] L. Zhou, F. Yang, and H. Zhou, "A novel efficient nonstandard high-order finite-difference time-domain method based on dispersion relation analysis," *Electromagnetics*, vol. 35, no. 1, pp. 59–74, 2015.
[6] M. F. Hadi and M. Piket-May, "A modified FDTD (2, 4) scheme for modeling electrically large structures with high-phase accuracy," *IEEE Transactions on Antennas and Propagation*, vol. 45, no. 2, pp. 254–264, 1997.
[7] J. B. Cole, "High accuracy solution of Maxwell's equations using nonstandard finite differences," *Computers in Physics*, vol. 11, no. 3, pp. 287–292, 1997.
[8] ——, "A high-accuracy realization of the Yee algorithm using non-standard finite differences," *IEEE Transactions on Microwave Theory and Techniques*, vol. 45, no. 6, pp. 991–996, 1997.
[9] T. Ohtani, K. Taguchi, T. Kashiwa, Y. Kanai, and J. B. Cole, "Non-standard FDTD method for wideband analysis," *IEEE Transactions on Antennas and Propagation*, vol. 57, no. 8, pp. 2386–2396, 2009.
[10] G. Sun and C. W. Trueman, "Unconditionally stable crank-nicolson scheme for solving two-dimensional Maxwell's equations," *Electronics Letters*, vol. 39, no. 7, pp. 595–597, 2003.
[11] Y. Yang, R. S. Chen, and E. K. N. Yung, "The unconditionally stable Crank-Nicolson FDTD method for three-dimensional Maxwell's equations," *Microwave and Optical Technology Letters*, vol. 48, no. 8, pp. 1619–1622, 2006.
[12] W. Chen, P. Ma, and J. Tian, "A novel ADE-CN-FDTD with improved computational efficiency for dispersive media," *IEEE Microwave and Wireless Components Letters*, vol. 28, no. 10, pp. 849–851, 2018.
[13] T. Namiki, "A new FDTD algorithm based on alternating-direction implicit method," *IEEE Transactions on Microwave Theory and Techniques*, vol. 47, no. 10, pp. 2003–2007, 1999.
[14] S. J. Cooke, M. Botton, T. M. Antonsen, Jr., and B. Levush, "A leapfrog formulation of the 3-D ADI-FDTD algorithm," *International Journal of Numerical Modelling Electronic Networks, Devices and Fields*, vol. 22, no. 2, pp. 187–200, 2008.
[15] X. Wang, W. Yin, and Z. Z. D. Chen, "One-step leapfrog ADI-FDTD method for simulating electromagnetic wave propagation in general dispersive media," *Optics Express*, vol. 21, no. 18, pp. 20 565–20 576, 2013.
[16] G. Xie, Z. Huang, M. Fang, and X. Wu, "A unified 3-D ADI-FDTD algorithm with one-step leapfrog approach for modeling frequency-dependent dispersive media," *International Journal of Numerical Modelling Electronic Networks, Devices and Fields*, vol. 33, no. 2, p. e2666, 2020.

**Harune Sekido** received her B. E. degree in electrical engineering, electronics, and information engineering from Nagoya University, Nagoya, Japan, in 2022. She is currently working toward the M.E. degree in electrical engineering at Nagoya University, Nagoya, Japan. Her research interests include computational sciences with application to electromagnetic wave.

**Takayuki Umeda** (M'22) received his B.E. degree in electrical and electronic engineering from Kyoto University, Kyoto, Japan, in 1999, and M.Inf. and Ph.D. degree in communications and computer engineering from Kyoto University, Kyoto, Japan, in 2001 and 2004, respectively. He is currently an Associate Professor with Institute for Space-Earth Environmental Research, Nagoya University, Nagoya, Japan. His research interests include computational sciences and high-performance computing with application to space plasma physics.